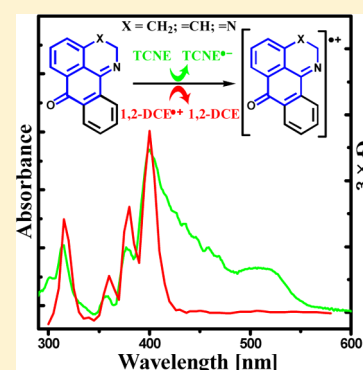


# Spectral and Kinetic Properties of Radical Cations Derived from Oxoisoaporphines: Relevance to Electron-Transfer Processes Involving Phytoalexins

Julio R. De la Fuente,<sup>\*,†</sup> Gabriel Kciuk,<sup>‡</sup> Christian Aliaga,<sup>†</sup> and Krzysztof Bobrowski<sup>\*,‡</sup><sup>†</sup>Departamento de Química Orgánica y Físicoquímica, Facultad de Ciencias Químicas y Farmacéuticas, Universidad de Chile, Casilla 223, Santiago 1, Chile<sup>‡</sup>Centre of Radiation Research and Technology, Institute of Nuclear Chemistry and Technology, 03-195 Warsaw, Poland

## S Supporting Information

**ABSTRACT:** The thermally induced intermolecular electron transfer reaction in acetonitrile between the tetracyanoethylene (TCNE), a  $\pi$ -electron acceptor with a large electron affinity, and six oxoisoaporphines (2,3-dihydro-7*H*-dibenzo[*de,h*]quinolin-7-one, 5-methoxy-2,3-dihydro-7*H*-dibenzo[*de,h*]quinolin-7-one, 1-azabeno[*de*]anthracen-7-one, 5-methoxy-1-azabeno[*de*]anthracen-7-one, 7*H*-benzo[*e*]perimidin-7-one, and 2-methyl-7*H*-benzo[*e*]perimidin-7-one) is reported. Spectral and kinetic characteristics are presented for radical cations derived from these six oxoisoaporphines either generated by a thermal reaction or generated radiolytically in argon-saturated 1,2-dichloroethane, oxygen-saturated acetone, and acetonitrile. The radical cations of oxoisoaporphines are insensitive to oxygen and are mostly characterized by absorption maxima of their most intense bands located at  $\lambda_{\text{max}} = 400\text{--}410$  nm, except of the radical cations derived from 2,3-dihydrooxoisoaporphines. For the latter compounds, the absorption maxima of the most intense absorption bands are located at  $\lambda_{\text{max}} = 290\text{--}295$  nm. Their locations are independent of the presence of functional groups and the solvents used. They are formed in bimolecular processes with pseudo-first-order rate constants ranging from  $2.1 \times 10^5$  to  $1.5 \times 10^6$  s<sup>-1</sup> (in solutions containing  $10^{-4}$  M of the substrate), depending on the derivative and the solvent used. They are stable either when formed via the electron-transfer reaction with TCNE or when generated in isolation in pulse radiolysis of Ar-saturated 1,2-dichloroethane. In acetone and acetonitrile they decay predominantly by first-order kinetics with the first-order rate constants ranging from  $2.3 \times 10^4$  to  $5.1 \times 10^4$  s<sup>-1</sup>. Formation of dimeric radical cations for all of the oxoisoaporphines studied was observed in acetonitrile solutions, and for azaoxoisoaporphines also in acetone solutions. The experimental spectra show a reasonably good agreement with the ZINDO/S semiempirical quantum mechanical calculations of radical cation absorptions.



## INTRODUCTION

Oxoisoaporphines, azaoxoisoaporphines, and oxoaporphines are alkaloids structurally related to phenalenones.<sup>1–4</sup> They have been isolated from above-ground parts of plants belonging to different families such as *Annonaceae*,<sup>5,6</sup> *Lauraceae*,<sup>7</sup> *Magnoliaceae*,<sup>8</sup> *Fumariaceae*,<sup>9,10</sup> *Menispermaceae*,<sup>11–14</sup> and *Papaveraceae*.<sup>15,16</sup> Of these three alkaloid families (oxoisoaporphines, azaoxoisoaporphines, and oxoaporphines) only the last has thus far been positively identified as phototoxic phytoalexins.<sup>1,2,17</sup> Phototoxicity of these compounds had been attributed mainly to its <sup>1</sup>O<sub>2</sub> generation.<sup>1</sup> They are synthesized by plants as a defense against pathogen agents or mechanical injury. For instance, oxoglucine is a phytoalexin from the *Magnoliaceae* family that is elicited in the plant after mechanical injury but its reduced form, glucine, is present in healthy plants.<sup>8</sup> Upon mechanical injury, glucine is rapidly oxidized to oxoglucine *in planta* via chemical (enzymatic oxidation) and photooxidation processes, in particular by <sup>1</sup>O<sub>2</sub>.<sup>16–18</sup>

Two mechanisms of phototoxin action have been proposed: (i) a direct photooxidation of biologically relevant molecules by

either electron or hydrogen abstraction and a subsequent reaction of the radical species formed with nearby oxygen molecules (type I mechanism) or (ii) an electronic excitation energy transfer from the phototoxin to molecular oxygen to form <sup>1</sup>O<sub>2</sub> (type II mechanism).<sup>19</sup> There is no doubt that formation of radical ions (radical cations, in particular) derived from these alkaloids should accompany electron-transfer reactions. Therefore, spectral and kinetic properties of oxoisoaporphine radical cations might be of relevance to electron-transfer processes occurring in phytoalexins and connected potentially with their activity against pathogens.

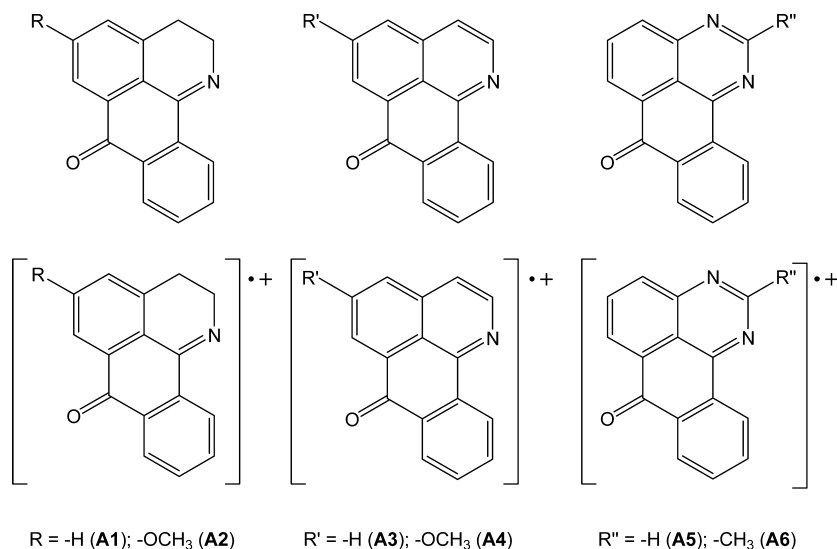
Some derivatives of these phenalenones-like alkaloids, especially those of 7*H*-benzo[*e*]perimidin-7-one containing two N atoms, have received considerable attention due to their antineoplastic activity and cytotoxicity against different tumoral cell lines.<sup>20–24</sup> These compounds, synthesized as

Received: March 10, 2014

Revised: May 2, 2014

Published: May 6, 2014

Chart 1. Structures of Oxoisoaporphine Derivatives and Respective Radical Cations under Study



noncardiotoxic alternatives of anthraquinone antitumor drugs, exhibit *in vitro* and *in vivo* cytotoxic activity toward multidrug resistant cell lines.<sup>22,23</sup> It was claimed that they had poor oxidizing ability due to their low efficiency in stimulating oxygen radical formation caused by their low enzyme substrate properties toward NADH dehydrogenase.<sup>22–24</sup>

There have been only a few studies concerning the generation of radical ions from oxoisoaporphines.<sup>25–30</sup> The preliminary results, concerning radical cations derived from oxoisoaporphines, have been reported for 2,3-dihydrooxoisoaporphine (A1 in Chart 1) and its 5-methoxy derivative (A2 in Chart 1) in our earlier paper.<sup>26</sup> An influence of the methoxy substitution in the aromatic ring on the position of the absorption bands was observed. In  $O_2$ -saturated acetonitrile, the radical cations of A1 were characterized by a strong nondescript absorption band with no distinct  $\lambda_{max}$  in the range 350–450 nm (its principal absorption band is probably located at  $\lambda < 350$  nm). On the other hand, the radical cations of A2, under the same conditions, showed a maximum at  $\lambda_{max} = 420$  nm. The substantial red shift of the absorption maximum was rationalized by an increase of charge density due to the presence of a methoxy group. These experimental observations were confirmed by the ZINDO/S calculations of the most intense absorption for both radical cations.<sup>26</sup>

In the present work we have undertaken a detailed study of the spectral and kinetic behavior of radical cations derived from six oxoisoaporphines (A1–A6) (Chart 1) produced as a result of thermal electron-transfer reactions between them and TCNE in acetonitrile (Experimental Procedures).

Various types of reactions between electron donors of low ionization potential and acceptors of large electron affinity, i.e.,  $\pi$ -electron acceptors, have been reported.<sup>31,32</sup> Some of them involved electron-donor–acceptor (EDA) complexes [D, A],<sup>33–36</sup> which were the precursors for the generation of “radical ion pairs” [D $^{\bullet+}$ , A $^{\bullet-}$ ] obtained by either one-electron chemical or photosensitized oxidations. The EDA complexes [D, A], may coexist in equilibrium with the charge-transfer complexes [D $^{\bullet+}$ , A $^{\bullet-}$ ]. The latter may be present either in the form of a contact radical ion pair (CRIP) or in strongly polar solvents, e.g., acetonitrile, as a solvent separated radical ion pair (SSRIP).<sup>37,38</sup>

Additional insight into the details of the oxidation mechanism of oxoisoaporphines (A1–A6, Chart 1) was gained by comparing the spectral and kinetic behaviors of radical cations derived from oxoisoaporphines formed as a result of radiation-induced charge transfer between oxoisoaporphines and radical cations derived from organic solvents of various polarity (1,2-dichloroethane (1,2-DCE), acetone, and acetonitrile). These solvents are well-known for pulse radiolysis generation of radical cation precursors.<sup>39</sup> We have initiated primarily this study to generate isolated oxoisoaporphine radical cations and to study their spectra and kinetic behavior. Semiempirical quantum mechanical calculations PM3 and ZINDO/S have been performed to assist in the interpretation of the data and compared with the spectra obtained in the thermally induced and radiation-induced reactions.

## EXPERIMENTAL PROCEDURES

**Materials.** All the chemical compounds used for the experiments were of the purest commercially available grade and were used as received. Acetonitrile (HPLC grade), acetone (99.7% purity with <0.2% of water), and 1,2-DCE (>99% purity) were purchased from J. T. Baker or Merck and from Sigma-Aldrich, respectively.

**Synthesis of Oxoisoaporphines.** 2,3-Dihydro-7*H*-dibenzo[*de,h*]quinolin-7-one (A1, Chart 1), 5-methoxy-2,3-dihydro-7*H*-dibenzo[*de,h*]quinolin-7-one (A2, Chart 1), 1-azabenz[*de*]anthracen-7-one (A3, Chart 1), and 5-methoxy-1-azabenz[*de*]anthracen-7-one (A4, Chart 1) were obtained by the procedure reported by Fabre et al.<sup>40</sup> and by Walker et al.,<sup>41</sup> and completely characterized as reported previously.<sup>42–44</sup>

Synthesis of 7*H*-benzo[*e*]perimidin-7-one (A5, Chart 1) and its 2-methyl substituted derivative, 2-methyl-7*H*-benzo[*e*]perimidin-7-one (A6, Chart 1) was performed by cyclization of 1-aminoanthraquinone either with *N,N*-dimethylformamide dimethylacetal or with *N,N*-dimethylacetamide dimethylacetal with phosphorus oxy chloride, respectively. In situ cyclization of the intermediates formed was accomplished by an addition of ammonium acetate in hot ethanol.<sup>20,23</sup>

**Preparation of Solutions.** All solutions for thermal generation of radical cations were prepared in square quartz cells and contained  $10^{-4}$  M of oxoisoaporphines with  $10^{-2}$  M TCNE in 3 mL of acetonitrile. Cells were provided with a

magnetic stirrer to ensure homogeneity of solutions during the experiments. All experiments were performed at 25 °C, except for azaoxoisoporphine A5, performed at 50 °C.

All solutions for pulse radiolysis experiments were prepared freshly before experiments with organic solvent and contained  $10^{-4}$  M of the oxoisoporphines. Acetonitrile and acetone solutions were subsequently purged for at least 30 min per 200 mL of sample with O<sub>2</sub> and 1,2-DCE solutions with Ar before irradiation.

**UV–Vis Spectrophotometry.** Changes in the absorbance occurring during thermal reactions between the respective oxoisoporphines and TCNE were monitored using a diode array spectrophotometer UV–visible 8453 Agilent. Due to the small changes in absorbances observed during the experiments, the absorbances measured at time  $t = 0$  were taken as the spectral blank, and the spectra measured thus constitute the difference between the absorbances measured at time  $t = t_n$  and  $t = 0$ . Such an experimental approach allowed us to appreciate small differences in absorbances measured, thus recording absorption bands of the products.

**Oxidation by Tetracyanoethylene (TCNE).** The tetracyanoethylene (TCNE), a  $\pi$ -acceptor of electrons with a reduction potential  $E_{\text{red}} = 0.24$  V vs SCE,<sup>45</sup> which is equivalent to a reduction potential,  $E_{\text{red}} = 0.48$  V vs NHE,<sup>46</sup> forms stable radical anions in solutions that can be isolated as salts. Electron-transfer reactions involving TCNE and suitable electron donors are usually fast enough and can be easily observed. Therefore, TCNE has been widely used in either thermal (involving EDA complexes)<sup>37,38,45,47,48</sup> or photochemical<sup>49–52</sup> generation of oxidized species such as radical cations and/or neutral species derived from various organic compounds.

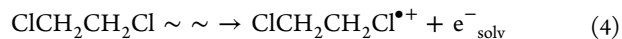
In the presence of an appropriate substrate, the radical anion, TCNE<sup>•-</sup>, characterized by a broad structured absorption band centered at  $\lambda = 425$  nm, can be generated by an electron transfer from a substrate to TCNE (eq 1).<sup>46,53–56</sup> The radical anion (TCNE<sup>•-</sup>), in a recombination reaction, is able to form the diamagnetic dimeric anion (TCNE)<sub>2</sub><sup>2-</sup>, (eq 2), absorbing between 450 and 600 nm,<sup>57,58</sup> and a paramagnetic dimeric radical anion ((TCNE)<sub>2</sub><sup>•-</sup>) (eq 3), absorbing in the near IR over 1000 nm,<sup>46,53–56</sup> in a reaction with an excess of TCNE. Although, the latter species should be the predominant in our experimental conditions, it was not spectrally accessible for us.



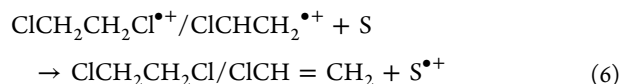
**Pulse Radiolysis.** Pulse radiolysis experiments were performed using a pulse radiolysis setup based on the 10 MeV electron linear accelerator (LAE 10) at the INCT with typical pulse lengths of 7–10 ns. The data acquisition system allows for kinetic traces to be displayed on multiple time scales. A detailed description of the experimental setup for optical measurements has been given elsewhere along with the basic details of the equipment and the data collection system.<sup>59,60</sup> The irradiation cell was supplied with a fresh solution by continuous and controlled flow. The dose per pulse determined by thiocyanate dosimetry was on the order of 18–20 Gy (1 Gy = 1 J kg<sup>-1</sup>). Radiolytic yields are given in SI units as  $\mu\text{mol J}^{-1}$ , i.e., the number of product species in micromoles that are generated for every joule of energy absorbed by the solution.

All experiments were performed with a continuous flow of sample solutions at room temperature ( $\sim 20$  °C). Experimental error limits are  $\pm 10\%$  unless specifically noted.

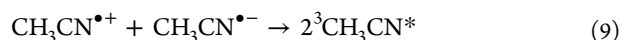
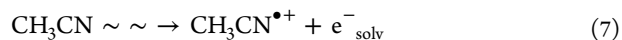
**Radiolysis of 1,2-DCE.** Pulse irradiation of Ar-saturated 1,2-DCE leads to the 1,2-DCE-derived radical cation and solvated electrons (eq 4). In 1,2-DCE, the solvated electrons do not persist because of the dissociative capture by the parent 1,2-DCE molecule (eq 5).



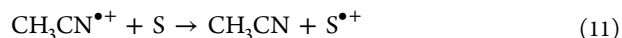
The 1,2-DCE-derived radical cations remain available for diffusional charge transfer to an added solute (eq 6). Two kinetically distinct cationic species have been implicated, namely, a radical cation (assigned as ClCH<sub>2</sub>CH<sub>2</sub>Cl<sup>•+</sup> or ClCHCH<sub>2</sub><sup>•+</sup> with  $G = 0.07$   $\mu\text{mol J}^{-1}$ ) and a carbocation (assigned as ClCH<sub>2</sub>CH<sub>2</sub><sup>+</sup> in either linear or cyclic chloronium cation form with  $G = 0.02$   $\mu\text{mol J}^{-1}$ ).<sup>61</sup>



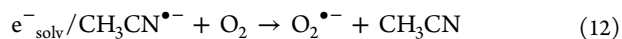
**Radiolysis of Acetonitrile.** Pulse irradiation of Ar-saturated neat acetonitrile leads to the formation of the acetonitrile positive ions and electrons/negative ions (eqs 7 and 8). Triplet states are also formed by a solute radical ion recombination (eqs 9 and 10). Low yields of  $G$  ( $\sim 0.02$   $\mu\text{mol J}^{-1}$ ) for the oxidizing species<sup>62</sup> and  $G$  ( $\sim 0.03$   $\mu\text{mol J}^{-1}$ ) for the triplets<sup>63,64</sup> were measured. On the other hand, the yield of reducing species was found in the range of  $G = 0.1067$ – $0.1606$   $\mu\text{mol J}^{-1}$ .<sup>64,65</sup>



When this solvent is O<sub>2</sub>-saturated, only radical cations of a solute are formed (ionization potential of CH<sub>3</sub>CN is  $\approx 12$  eV)<sup>66</sup> (eq 11).

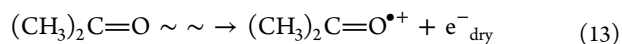


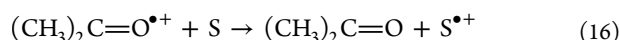
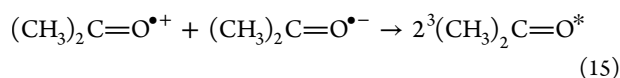
Solute radical anions are not formed because their precursors, solvated electrons and/or solvent radical anions, are scavenged by O<sub>2</sub> (eq 12).



Oxygen also serves as a strong quencher for the triplets of solutes and solvents.

**Radiolysis of Acetone.** Pulse irradiation of Ar-saturated acetone leads to relatively long-lived radical ions (eqs 13 and 14) and triplet states (formed via geminate recombination, eq 15).<sup>67–70</sup> The free ions and triplet yields were measured to be 0.078 and 0.104  $\mu\text{mol J}^{-1}$ , respectively.<sup>71</sup> Of particular interest in the present study is the molecular radical cation of acetone that is involved in charge transfer to a solute that leads to the respective radical cation (eq 16).





In  $\text{O}_2$ -saturated acetone only radical cations of a solute ( $\text{S}^{\bullet+}$ ) are formed. Solute radical anions ( $\text{S}^{\bullet-}$ ) are not formed because their precursors, acetone radical anions ( $(\text{CH}_3)_2\text{C}=\text{O}^{\bullet-}$ ), are scavenged (similar to the behavior in acetonitrile, *vide supra*) by  $\text{O}_2$ . Oxygen also serves as a strong quencher for the triplets of solutes and solvents.

**Quantum Mechanical Calculations.** Calculated spectra employing the PM3 minimized geometries for isolated oxoisoaporphine-derived radical cations were obtained by using ZINDO/S, by considering 10 + 10 excited states IC single point ZINDO/S method.

For the oxoisoaporphine radical cation dimers, the optimized structures of the ground state molecule and the respective radical cation were merged together and optimized by using molecular mechanic  $\text{MM}^+$  to obtain the dimer structures. These structures were optimized at the PM3 level, and finally the spectra were calculated by a single point IC ZINDO/S using the orbital criterion taking 10 + 10 orbital. All calculations were done by using HyperChem 8.0.

## RESULTS AND DISCUSSION

**2,3-Dihydrooxoisoaporphines, A1 and A2.** *2,3-Dihydro-7H-dibenzo[de,h]quinolin-7-one (A1)*. Mixing of acetonitrile solutions containing separately TCNE and A1 generates significant changes in the UV–vis spectra with the evolution of time on the minute time domain. A well-resolved band with  $\lambda_{\text{max}} = 295$  nm appeared together with a broad band between 320 and 450 nm and a second one, less intense, centered at  $\lambda_{\text{max}} = 515$  nm (Figure 1A). These spectral changes can be tentatively attributed to the formation of  $\text{A1}^{\bullet+}$  and the TCNE radical anion,  $\text{TCNE}^{\bullet-}$ , formed according to eq 1 (Experimental Procedures). The first species was characterized by a broad absorption band ranged between 370 and 410 nm,<sup>26</sup> and the second one by a structured absorption band centered at  $\lambda_{\text{max}} = 425$  nm, respectively.<sup>46,53–56</sup>

A broad absorption band located between 450 and 600 nm can be assigned to the diamagnetic dimeric anion  $(\text{TCNE})_2^{\bullet-}$ , which is formed according to eq 2 (Experimental Procedures).<sup>57,58</sup> Thus, the presence of this species is additional evidence for the formation, albeit indirect, of  $\text{A1}^{\bullet+}$ .

Interestingly, absorbances recorded at  $\lambda = 295$ , 350, and 415 nm showed similar temporal behaviors (Figure 1A, inset), however, different from that recorded at  $\lambda = 515$  nm. This observation clearly showed that absorption bands of radical cations  $\text{A1}^{\bullet+}$  and  $\text{TCNE}^{\bullet-}$  radical anions located in the spectral region between 295 and 415 nm were formed simultaneously according to eq 1. On the other hand, different temporal behavior observed at  $\lambda = 515$  nm and characterized by a plateau established after 10 min following the mixing of solutions confirms the formation of another species, i.e., the diamagnetic dimeric anion  $(\text{TCNE})_2^{\bullet-}$ .

Moreover, semiempirical quantum mechanical calculations for the radical cation  $\text{A1}^{\bullet+}$  predicted a strong absorption in the 325 nm region and less intense absorption between 370 and 430 nm, thus showing a fairly good agreement with the experimental spectra shown in Figure 1A.

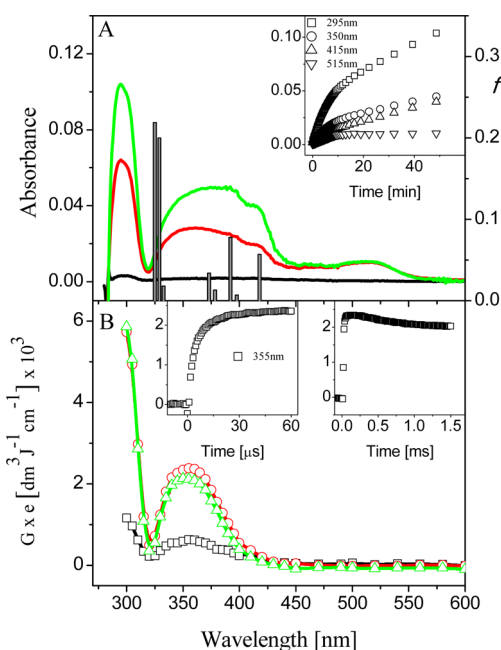


**Figure 1.** (A) Absorption spectra for the reaction mixture containing A1/TCNE in Ar-saturated acetonitrile at time  $t = 0$  (black), 15 (red), and 50 min (green). The shaded vertical bars represent position and oscillator strength ( $f$ ) of the calculated electronic transitions for  $\text{A1}^{\bullet+}$ . Inset: temporal evolution of absorbances recorded at different wavelengths. (B) Transient absorption spectra observed 1  $\mu\text{s}$  ( $\square$ ), 120  $\mu\text{s}$  ( $\circ$ ), and 1 ms ( $\triangle$ ) after pulse irradiation of an Ar-saturated 1,2-DCE solution containing  $1 \times 10^{-4}$  M of A1. Insets: time profiles representing a growth and decay at  $\lambda = 355$  nm at different time scales (Note: In this and all the following graphics, the insets' y-axes have the same units as in the main plots).

Pulse radiolysis of Ar-saturated 1,2-DCE solutions containing A1 led to a transient absorption spectrum that was fully developed within the range of 100  $\mu\text{s}$  (Figure 1B, inset). The spectrum consisted of a distinctive absorption band with  $\lambda_{\text{max}} = 355$  nm and a strong nondescript absorption band with  $\lambda_{\text{max}}$  located below 300 nm (Figure 1B). It is noteworthy that for this solvent it was possible to extend optical measurements down to 300 nm, contrary to acetonitrile<sup>26</sup> and acetone solutions (*vide infra*). These two bands were identical with those obtained via a thermal reaction of A1 with TCNE (Figure 1A). Therefore, we assigned the 295 and 355 nm bands to  $\text{A1}^{\bullet+}$ . The most reasonable precursor responsible for its formation is the solvent radical cation  $\text{ClCH}_2\text{CH}_2\text{Cl}^{\bullet+}$  (eq 17).



The absorption trace recorded at 355 nm was stable over the time domain of 200  $\mu\text{s}$  and slowly decayed over the submillisecond time domain (Figure 1B, right inset).

Pulse radiolysis of a solution of A1 in  $\text{O}_2$ -saturated acetone (Figure S1 in the Supporting Information) yielded a spectrum with features similar to those observed earlier by us in oxygen-saturated acetonitrile solutions.<sup>26</sup> The absorption spectrum recorded at 10  $\mu\text{s}$  exhibited a strong nondescript absorption band with no distinct  $\lambda_{\text{max}}$  at the wavelengths in the range 350–650 nm. The 350 nm band was fully developed within the range of 10  $\mu\text{s}$ , and the formation kinetics recorded at  $\lambda = 350$  nm with  $k = (2.2 \pm 0.6) \times 10^5 \text{ s}^{-1}$  were slightly slower than the analogous formation kinetics in  $\text{O}_2$ -saturated acetonitrile ( $k = 3.8 \pm 0.04) \times 10^5 \text{ s}^{-1}$ .<sup>26</sup> Reasonably, the radical cation  $\text{A1}^{\bullet+}$  is

responsible for the absorption below 390 nm. With a further lapse of time, the absorption in the region of 350–650 nm decreased in intensity, however, not uniformly. The decay kinetics observed at  $\lambda = 420$  and 500 nm were slightly slower than that observed at  $\lambda = 350$  nm. This observation resembled the spectral and kinetic features recorded earlier in  $O_2$ -saturated acetonitrile,<sup>26</sup> however, in not so distinctly a pronounced way. Very plausibly, it might suggest an involvement of a dimeric radical cation ( $(A1)_2^{\bullet+}$ ) formed as the product of an association of  $A1^{\bullet+}$  and its parent A1 molecule (eq 18).



*5-Methoxy-2,3-dihydro-7H-dibenzo[de,h]quinolin-7-one* (A2). Similarly, as for A1, mixing of acetonitrile solutions containing separately A2 and TCNE resulted in an appearance of two strong absorption bands with  $\lambda_{\max} = 290$  and 415 nm, which can be tentatively attributed to the radical cation  $A2^{\bullet+}$  and the TCNE $^{\bullet-}$  radical anion (Figure 2A).

A weakly developed absorption band with  $\lambda_{\max} = 345$  nm can be attributed to  $A2^{\bullet+}$ , on the basis of the spectral features of  $A2^{\bullet+}$  observed in 1,2-DCE solutions (*vide infra*). Moreover, it is reasonable to assume that two additional absorption maxima observed in 1,2-DCE and assigned to  $A2^{\bullet+}$  were masked by a strong absorption caused by the presence of the TCNE $^{\bullet-}$  radical anion. The very low intensity of the absorption band with  $\lambda = 515$  nm showed a very small contribution from (TCNE) $_2^{2-}$ . Both bands at  $\lambda = 290$  and 415 nm grew with a similar rate constant ( $k = (4.4 \pm 0.04) \times 10^{-4} \text{ s}^{-1}$ ).

Similarly, as for A1, the transient absorption spectra obtained after electron irradiation in Ar-saturated 1,2-DCE containing A2 were slow to develop and reached a plateau within the range of hundreds of microseconds (Figure 2B). The absorption spectrum was characterized by three distinct absorption maxima located at  $\lambda_{\max} = 345$ , 385, and 405 nm. Within the first 20  $\mu\text{s}$  after the pulse the absorption spectrum started to form uniformly at all wavelengths. The absorbances recorded at  $\lambda = 345$ , 385, and 405 nm grew nearly with the same rate constant  $k = (2.1 \pm 0.03) \times 10^5 \text{ s}^{-1}$ . This indicates that all three absorption maxima can be attributed to the same transient species  $A2^{\bullet+}$ . Moreover, these absorptions were reasonably well reproduced by the ZINDO/S calculation for  $A2^{\bullet+}$ , as shown by the bars in Figure 2B. Interestingly, within the 20–300  $\mu\text{s}$  time domain the absorbances at  $\lambda_{\max}$  continued to increase further without forming any new absorption bands. This last observation suggests that radical cations of A2 ( $A2^{\bullet+}$ ) are formed in 1,2-DCE via two independent processes.

Similar transient absorption spectra were observed in  $O_2$ -saturated acetonitrile,<sup>26</sup> and acetone solutions (Figure 2C). A transient absorption spectrum recorded 6  $\mu\text{s}$  after the electron pulse in acetone solutions was dominated by a distinctive absorption band with  $\lambda_{\max} = 410$  nm with two weakly developed narrow blue- and red-edge shoulders in the range of 385–395 and 440–460 nm, respectively (Figure 2C). The formation kinetics recorded at  $\lambda = 415$  nm with  $k = (5.8 \pm 0.7) \times 10^5 \text{ s}^{-1}$  were slightly faster than the analogous formation kinetics in  $O_2$ -saturated acetonitrile ( $k = 4.6 \pm 0.09) \times 10^5 \text{ s}^{-1}$ .<sup>26</sup> The region below  $\lambda = 350$  nm was not accessible for measurements due to a strong absorption of the parent compound and the solvent. It is noteworthy that, with the further lapse of time, the absorption spectrum decayed uniformly at all wavelengths suggesting a very small, if any, contribution from the dimeric species  $(A2)_2^{\bullet+}$  in acetone. These transient spectra were very similar to the analogous

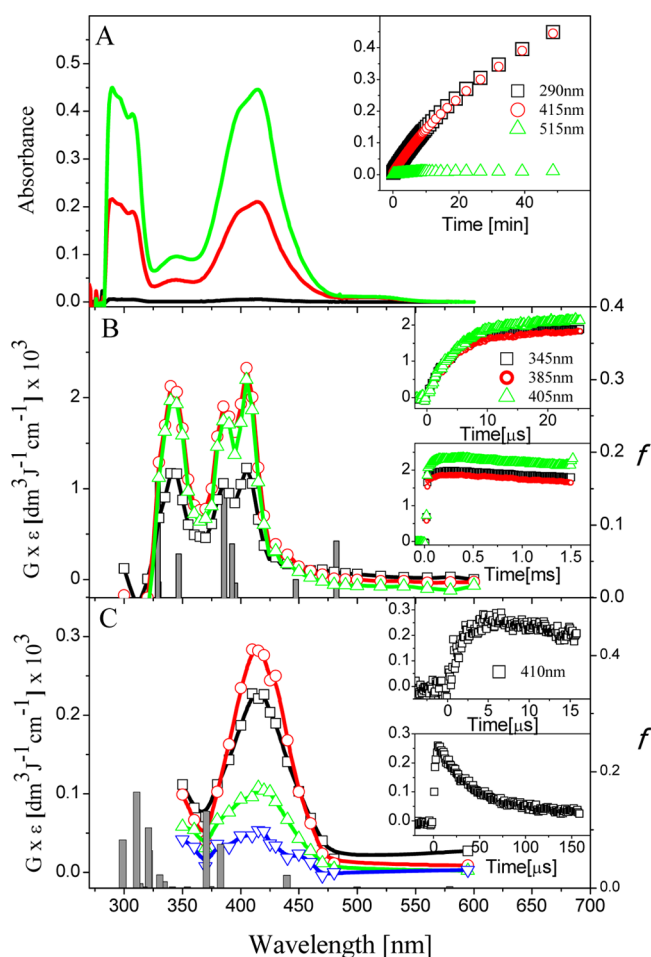


**Figure 2.** (A) Absorption spectra for the reaction mixture containing A2/TCNE in Ar-saturated acetonitrile at time  $t = 0$  (black), 15 (red), and 50 min (green). The inset shows the kinetic profiles at different wavelengths. (B) Transient absorption spectra observed at 4  $\mu\text{s}$  ( $\square$ ), 240  $\mu\text{s}$  ( $\circ$ ), and 1 ms ( $\triangle$ ) after pulse irradiation of an Ar-saturated 1,2-DCE solution containing  $1 \times 10^{-4}$  M of A2. Insets: time profiles recorded at different wavelengths. The shaded vertical bars represent the position and oscillator strength ( $f$ ) of the calculated electronic transitions for  $A2^{\bullet+}$ . (C) Transient absorption spectra observed at 2 ( $\square$ ), 6 ( $\circ$ ), 60 ( $\triangle$ ), and 120  $\mu\text{s}$  ( $\nabla$ ) after pulse irradiation of an  $O_2$ -saturated acetone solution containing  $1 \times 10^{-4}$  M of A2. Insets: time profiles recorded at  $\lambda = 410$  nm ( $\square$ ). The shaded vertical bars represent the position and oscillator strength ( $f$ ) of the calculated electronic transitions for  $(A2)_2^{\bullet+}$ .

spectrum recorded earlier in  $O_2$ -saturated acetonitrile and assigned by us to the radical cation derived from A2 ( $A2^{\bullet+}$ , Chart 1),<sup>26</sup> and to those obtained in the presence of TCNE, Figure 2A.

The spectral differences between these spectra obtained by different techniques are expected, due to the solvents used and the presence of several TCNE species in the thermal experiments. Moreover, a substantial influence of the substitution with the methoxy group in the position 5 of the aromatic ring on the location of the maxima of  $A1^{\bullet+}$  and  $A2^{\bullet+}$  observed earlier in acetonitrile was also clearly seen in acetone and dichloroethane with a red-shift of about 50 nm.

**Oxoisoaporphines, A3 and A4.** *1-Azabenz[de]-anthracen-7-one* (A3). Mixing of acetonitrile solutions containing separately A3 and TCNE solutions generated rapid changes in the spectra with the appearance of the

absorption band with  $\lambda_{\max} = 515$  nm, attributed to  $(\text{TCNE})_2^{2-}$ , and three distinctly developed bands with  $\lambda_{\max}$  located at 335, 387, and 408 nm. They can be attributed to the radical cation  $\text{A3}^{*\cdot}$ . Location of these absorption bands revealed a reasonably good correlation with the calculated electronic transitions for  $\text{A3}^{*\cdot}$ , albeit the lower energy transitions were not observed (Figure 3A). It is noteworthy that the absorptions between 335 and 408 nm grew with a similar rate constant  $k = (2.0 \pm 0.06) \times 10^{-4} \text{ s}^{-1}$  (insert in Figure 3A).

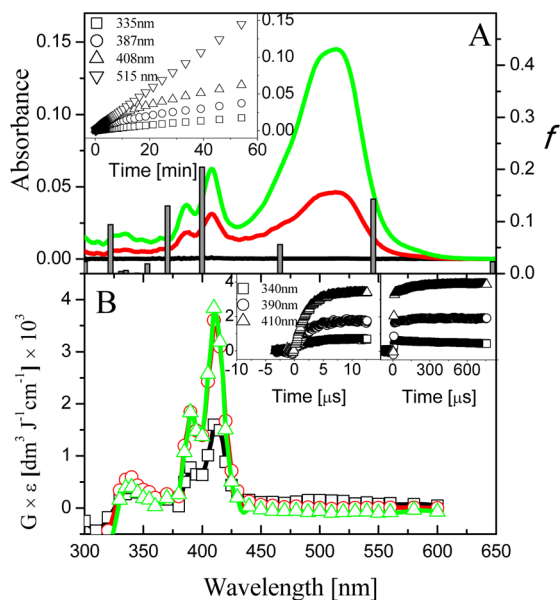


**Figure 3.** (A) Absorption spectra for the reaction mixture containing  $\text{A3}/\text{TCNE}$  in Ar-saturated acetonitrile solutions at time  $t = 0$  (black), 15 (red), and 55 min (green). The inset shows the kinetic profiles at different wavelengths. The shaded vertical bars represent the position and oscillator strength ( $f$ ) of the calculated electronic transitions for  $\text{A3}^{*\cdot}$ . (B) Transient absorption spectra observed at 1.2  $\mu\text{s}$  ( $\square$ ), 100  $\mu\text{s}$  ( $\circ$ ), and 1 ms ( $\triangle$ ) after pulse irradiation of an Ar-saturated 1,2-DCE solution containing  $1 \times 10^{-4}$  M of  $\text{A3}$ . Insets: time profiles of the transient at different wavelengths.

Pulse radiolysis of Ar-saturated 1,2-DCE solutions containing  $10^{-4}$  M  $\text{A3}$  resulted in the appearance of the absorption spectra, which were very similar to those observed in the thermal reaction and assigned to  $\text{A3}^{*\cdot}$  (Figure 3B). The absorption spectrum recorded 100  $\mu\text{s}$  after the electron pulse exhibited two distinct albeit narrow absorption bands with  $\lambda_{\max} = 390$  and 410 nm. A weak absorption band with  $\lambda_{\max} = 340$  nm was also seen (Figure 3B). The formation of the more intense 410 nm band was fully developed within 12  $\mu\text{s}$  and matched the formation kinetics of the 390 nm band (Figure 3, left inset). The absorbances recorded at  $\lambda = 410$  and 390 nm grew with  $k = (2.3 \pm 0.05) \times 10^5 \text{ s}^{-1}$ . With the lapse of time, the spectra recorded did not change their spectral features significantly in the vicinity of the earlier observed absorption maxima. Interestingly, the 390 and 410 nm bands grew further over the 500  $\mu\text{s}$  time domain (Figure 3B, right inset); however, over the same time domain the 340 nm absorption band slowly disappeared (Figure 3B, right inset).

The transient absorption spectra recorded at various times after pulse irradiation of  $\text{O}_2$ -saturated acetone solution containing  $10^{-4}$  M  $\text{A3}$  are presented in Figure 4A. The absorption spectrum recorded at 8  $\mu\text{s}$  after the pulse exhibited

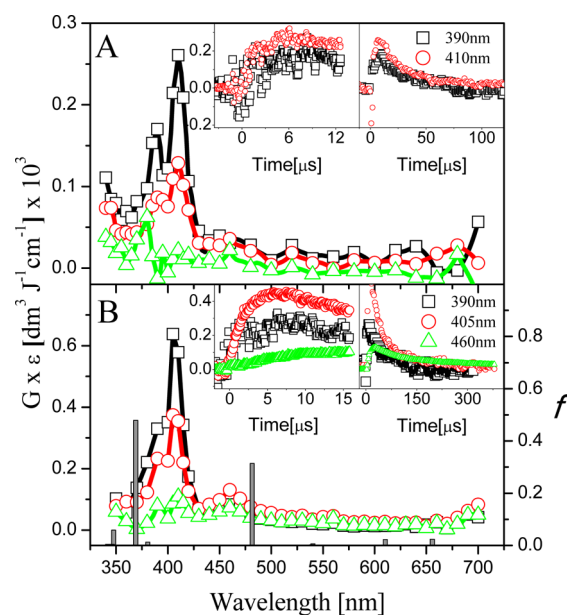


**Figure 4.** (A) Transient absorption spectra observed 8 ( $\square$ ), 24 ( $\circ$ ), and 100  $\mu\text{s}$  ( $\triangle$ ) after pulse irradiation of an  $\text{O}_2$ -saturated acetone solution containing  $1 \times 10^{-4}$  M of  $\text{A3}$ . Insets: time profiles of the transient at  $\lambda = 390$  and 410 nm. (B) Transient absorption spectra observed 6 ( $\square$ ), 25 ( $\circ$ ), and 100  $\mu\text{s}$  ( $\triangle$ ) after pulse irradiation of an  $\text{O}_2$ -saturated acetonitrile solution containing  $1 \times 10^{-4}$  M of  $\text{OIA}$ . Insets: time profiles of the transient at different wavelengths. The shaded vertical bars represent the position and oscillator strength ( $f$ ) of the calculated electronic transitions for  $(\text{A3})_2^{*\cdot}$ .

two absorption bands of various intensities with maxima located at  $\lambda_{\max} = 390$  and 410 nm (Figure 4A). The formation of the more intense 410 nm band was fully developed within 8  $\mu\text{s}$  and matched the formation kinetics of the 390 nm band. The absorbances recorded at  $\lambda = 410$  and 390 nm grew with  $k = (4.5 \pm 1.4) \times 10^5 \text{ s}^{-1}$ . This observation, taken together with the fact that decay kinetics observed at these two wavelengths were nearly similar, suggests the existence of only one species (Figure 4A, inset). Because the spectral features were very similar to those observed in 1,2 DCE solutions (Figure 3B), the spectrum was also assigned to  $\text{A3}^{*\cdot}$  (Chart 1).

Additional support for this assignment was obtained by comparison with the absorption spectra obtained after pulse irradiation of  $\text{O}_2$ -saturated acetonitrile solution containing  $10^{-4}$  M  $\text{A3}$  (Figure 4B). The transient absorption spectrum obtained 6  $\mu\text{s}$  after the pulse consisted of a strong absorption band with a maximum located at  $\lambda_{\max} = 405$  nm, a blue-edge shoulder in the 390–400 nm range, and a weak absorption band with  $\lambda_{\max} = 460$  nm (Figure 4B). The formation kinetics recorded at  $\lambda = 405$  nm with  $k = (5.7 \pm 0.2) \times 10^5 \text{ s}^{-1}$  nearly matched the formation kinetics at  $\lambda = 390$  nm. Interestingly, a third absorption band with  $\lambda_{\max} = 460$  nm developed further with  $k = (1.6 \pm 0.04) \times 10^5 \text{ s}^{-1}$  (Figure 4B, left inset). Moreover, the observed changes of the ratio  $r = G\epsilon_{405}/G\epsilon_{460}$  calculated at different lapsed times strongly suggest the presence of a second cationic species in acetonitrile. This statement is also consistent with the fact that decay kinetics observed at  $\lambda_{\max} = 405$  and 460 nm were also different, with the first-order rate constants  $k = (2.7 \pm 0.06) \times 10^4 \text{ s}^{-1}$  and  $k = (8.2 \pm 0.2) \times 10^3 \text{ s}^{-1}$ , respectively (Figure 4B, right inset). Therefore, the absorption band with  $\lambda_{\max} = 405$  nm and a blue-edge shoulder in 390–400 nm range are assigned to  $\text{A3}^{*\cdot}$ .

By analogy to acetonitrile solutions containing A1 and A2 (where 500 nm band developed at longer times after pulse irradiation)<sup>26</sup> the 460 nm band was tentatively assigned to a dimeric radical cation ((A3)<sub>2</sub><sup>•+</sup>) formed as a product of the association of A3<sup>•+</sup> and its parent molecule A3 (eq 19).



**5-Methoxy-1-azabenz[de]anthracen-7-one (A4).** The thermal reaction between A4 and TNCE showed nearly the same behavior when A3 was involved, with the fast appearance of the absorption band at  $\lambda_{\text{max}} = 515$  nm assigned to (TCNE)<sub>2</sub><sup>2-</sup>. Hence, the other absorption bands with maxima located at 340, 380, and 400 nm corresponds to A4<sup>•+</sup> (Figure S2A in the Supporting Information).

Pulse radiolysis of Ar-saturated 1,2-DCE solutions containing 10<sup>-4</sup> M A4 (Figure S2B in the Supporting Information) provided more arguments for the spectral assignment. The absorption spectrum recorded 12  $\mu\text{s}$  after the pulse exhibited three distinct albeit narrow absorption bands with  $\lambda_{\text{max}} = 345$ , 385, and 405 nm, matching almost exactly those obtained in the thermal process. The more intense 405 nm band was fully developed within 12  $\mu\text{s}$  and matched the formation kinetics of the 385 and 345 nm bands, with a rate constant  $k = (4.2 \pm 0.07) \times 10^5 \text{ s}^{-1}$ . With the lapse of time the spectra recorded did not change their spectral features significantly in the vicinity of the earlier observed absorption maxima. Similarly to 1,2-DCE solutions containing A3, the 385 and 405 nm bands grew further over the 500  $\mu\text{s}$  time domain while the 345 nm band slowly decayed.

More insight can be obtained from the spectral evolutions observed after irradiation in acetonitrile solution containing A4. They were similar to those observed for A1, A2, and A3. The transient absorption spectrum obtained 2  $\mu\text{s}$  after the pulse consisted of a strong absorption band located at  $\lambda_{\text{max}} = 400$  nm, a weaker blue-edge shoulder in the 370–400 nm range, and a red-edge shoulder in the range of 430–490 nm (Figure S2C in Supporting Information). With the further lapse of time, the absorption spectrum in the 350–430 nm region decreased in intensity; however, the spectra observed at 48  $\mu\text{s}$  after the pulse were characterized by a distinct absorption maximum at  $\lambda_{\text{max}} = 460$  nm (Figure S2C in the Supporting Information).

The formation kinetics recorded at  $\lambda = 400$  nm with  $k = (7.8 \pm 2.7) \times 10^5 \text{ s}^{-1}$  matched reasonably well the formation kinetics at  $\lambda = 370$  nm with  $k = (9.4 \pm 4.8) \times 10^5 \text{ s}^{-1}$ . Interestingly, a third absorption band with  $\lambda_{\text{max}} = 460$  nm developed further with  $k = (1.3 \pm 0.02) \times 10^5 \text{ s}^{-1}$  (Figure 4B, left inset). Again a close inspection of the spectra showed that the ratio  $r = G\epsilon_{400}/G\epsilon_{460}$  was not constant at times 2, 12, and 48  $\mu\text{s}$ . This observation, taken together with the fact that both the formation and decay kinetics observed at  $\lambda_{\text{max}} = 400$  and 460 nm were different, confirmed the existence of a dimeric radical cation (A4)<sub>2</sub><sup>•+</sup> formed as the product of the association of A4<sup>•+</sup> and its parent molecule, A4 (eq 20).



On the other hand, in O<sub>2</sub>-saturated acetone solution (data not shown), the transient absorption spectra with maxima located at  $\lambda_{\text{max}} = 380$  and a shoulder at 400 nm decreased uniformly in intensity and disappeared within 50  $\mu\text{s}$  after the pulse. This observation shows again the existence of only one species in acetone, namely A4<sup>•+</sup> (Chart 1), and the absence of any absorption band which might be assigned to the dimeric species (A4)<sub>2</sub><sup>•+</sup>.

**Azaoxisoorphines, A5 and A6. 7H-Benzo[e]-perimidin-7-one (A5).** The thermal reaction between A5 and TCNE showed spectral and kinetic features (Figure 5A) similar

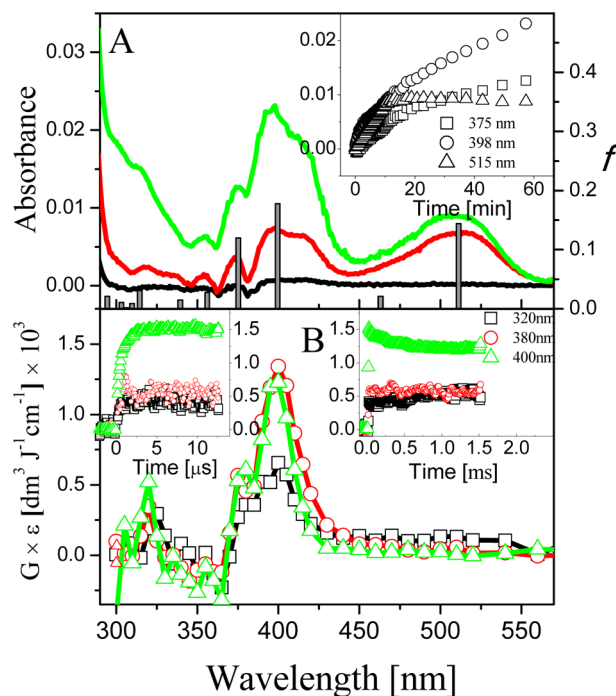


**Figure 5.** (A) Absorption spectra for the reaction mixture containing AS/TCNE in Ar-saturated acetonitrile at time  $t = 0$  (black), 10 (red), and 60 min (green). The inset shows the kinetic profiles at different wavelengths. The shaded vertical bars represent the position and oscillator strength ( $f$ ) of the calculated electronic transitions for AS<sup>•+</sup>. (B) Transient absorption spectra observed at 0.24 ( $\square$ ), 6 ( $\circ$ ), and 800  $\mu\text{s}$  ( $\triangle$ ) after pulse irradiation of an Ar-saturated 1,2-DCE solution containing 10<sup>-4</sup> M of AS. Insets: time profiles of the transient at  $\lambda = 320$ , 380, and 400 nm.

to those observed with the oxoisoorphines derivatives (A3 and A4) with the fast appearance of the absorption band at  $\lambda_{\text{max}} = 515$  nm assigned to (TCNE)<sub>2</sub><sup>2-</sup> and the structured shoulder ranged between 400 and 425 nm assigned to TCNE<sup>•-</sup>. A strong absorption band with  $\lambda_{\text{max}} = 398$  nm together with the weak absorption bands with  $\lambda_{\text{max}}$  at 375, 355, and 320 nm can be attributed to AS<sup>•+</sup>. Absorbances recorded at  $\lambda = 398$  and 375 nm showed similar temporal behaviors (Figure 5A, inset) confirming that these absorption bands can be attributed to the same species, namely AS<sup>•+</sup>. The calculated electronic transitions reproduced very well the absorption maxima observed at  $\lambda = 398$ , 375, 355, and 320 nm (Figure 5A).

Pulse radiolysis of Ar-saturated 1,2-DCE solutions containing 10<sup>-4</sup> M A5 resulted in the appearance of the absorption spectra (Figure 5B) that were very similar to those observed in Ar-saturated 1,2-DCE solutions containing A2–A4 derivatives (except A1). The absorption spectrum recorded 6  $\mu\text{s}$  after the pulse exhibited two distinct albeit narrow absorption bands with  $\lambda_{\text{max}} = 380$  and 400 nm, which matched closely those observed in the thermal reaction and the calculated spectra (Figure 5B). This includes the third absorption band with  $\lambda_{\text{max}} = 320$  nm, which was blue-shifted compared to A3<sup>•+</sup> and A4<sup>•+</sup>, and it also was well represented by calculations. The more intense 400 nm band was fully developed within 6  $\mu\text{s}$  with the first-order rate constant  $k = (1.5 \pm 0.04) \times 10^6 \text{ s}^{-1}$  and was

faster than those measured for A3 and A4. With a lapse of time up to 240  $\mu\text{s}$ , the absorption band with  $\lambda_{\text{max}} = 400$  nm remained constant and started to decay slowly over the millisecond time domain. These results corroborate the assignment of the observed spectra in the system containing A5/TCNE in acetonitrile to the radical cation  $\text{A5}^{\bullet+}$ .

Upon pulse radiolysis of an  $\text{O}_2$ -saturated acetone solution of  $10^{-4}$  M A5, a transient absorption was observed with two maxima located at  $\lambda_{\text{max}} = 400$  and 470 nm (Figure S3A in the Supporting Information). Interestingly, the kinetic traces recorded were characterized by distinctly different time profiles. The rates of formation and decay of the 400 nm absorption band were faster in comparison to those of the 470 nm absorption band (Figure S3A in the Supporting Information, insets). The 400 nm band was fully developed within the range of 2.4  $\mu\text{s}$  with the first-order rate constant  $k = (1.1 \pm 0.1) \times 10^6$   $\text{s}^{-1}$  while the 470 nm band was fully developed within the range of 8  $\mu\text{s}$  with the first-order rate constant  $k = (2.7 \pm 0.6) \times 10^5$   $\text{s}^{-1}$  (Figure S3A in the Supporting Information, left inset).

The 400 nm band decayed in a first-order process with  $k = (5.1 \pm 0.2) \times 10^4$   $\text{s}^{-1}$ , and a delayed decay of the 470 nm band was observed with  $k = (1.5 \pm 0.07) \times 10^4$   $\text{s}^{-1}$  (Figure S3A in the Supporting Information, right inset). Again a close inspection of spectra showed that the ratio  $r = G\epsilon_{400}/G\epsilon_{470}$  calculated at different times (0.6, 8, and 20  $\mu\text{s}$ ) was not constant. By analogy to similar observations in acetonitrile solutions, the most plausible interpretation appears to be in terms of existence of two different radical cationic species: the radical cation  $\text{A5}^{\bullet+}$  and the dimeric radical cation  $(\text{A5})_2^{\bullet+}$ .

The features of the spectral evolution in  $\text{O}_2$ -saturated acetonitrile solution containing A5 observed after irradiation were similar to those observed earlier for A1, A2, and A3. The transient absorption spectrum obtained 3.2  $\mu\text{s}$  after the pulse consisted of a strong absorption band located at  $\lambda_{\text{max}} = 400$  nm, a very narrow blue-edge shoulder in the 370–380 nm range and a red-edge shoulder in the range 430–470 nm (Figure S3B in the Supporting Information). The 400 nm band was developed with the first-order rate constant  $k = (9.8 \pm 0.3) \times 10^5$   $\text{s}^{-1}$  while the 440 nm band was fully developed with the first-order rate constant  $k = (3.2 \pm 0.3) \times 10^5$   $\text{s}^{-1}$  (Figure S3A in the Supporting Information, left inset).

While in the time range 3.2–20  $\mu\text{s}$  the absorption spectrum in the 350–430 nm region decreased with the rate constant  $k_{400} = (4.4 \pm 0.1) \times 10^4$   $\text{s}^{-1}$ , the intensity of the red-edge shoulder remained nearly constant. It started decaying on the submillisecond time domain with the rate constant  $k_{440} = (6.7 \pm 0.6) \times 10^3$   $\text{s}^{-1}$ . These observations suggest again the existence of two radical cationic species  $\text{A5}^{\bullet+}$  and  $(\text{A5})_2^{\bullet+}$  in acetonitrile.

**2-Methyl-7H-benzo[e]perimidin-7-one (A6).** The thermal reaction of A6 with TCNE revealed features similar to those observed with A5. A fast formation of partly overlapping absorption bands with  $\lambda_{\text{max}}$  at 315, 357, 377, 400, and 515 nm was produced (Figure 6A). A broad structured shoulder ranged between 420 and 480 nm and the absorption band with  $\lambda_{\text{max}} = 515$  nm were attributed to  $\text{TCNE}^{\bullet-}$  and  $(\text{TCNE})_2^{\bullet-}$ , respectively. The remaining absorption bands below 410 nm were assigned to  $\text{A6}^{\bullet+}$ . These absorptions closely match the calculated electronic transitions for  $\text{A6}^{\bullet+}$ ; however, the calculated electronic transitions at  $\lambda = 450$  and 500 nm were not present in 1,2-DCE solutions (Figure 6B).

Pulse radiolysis of Ar-saturated 1,2-DCE solutions containing  $10^{-4}$  M A6 resulted in the absorption spectra (Figure 6B) that were very similar to those formed during the thermal reaction

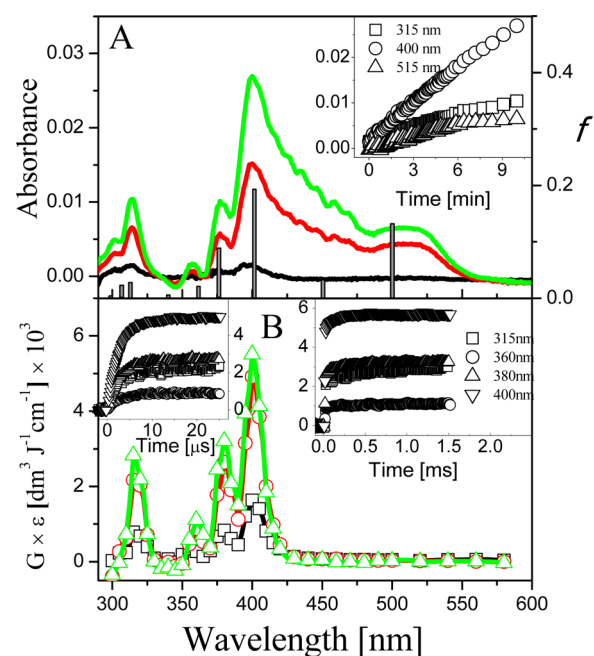


**Figure 6.** (A) Absorption spectra for the reaction mixture containing A6/TCNE in acetonitrile at time  $t = 0$  (black), 5 (red), and 10 min (green). The inset shows the kinetic profiles at different wavelengths. The shaded vertical bars represent the position and oscillator strength ( $f$ ) of the calculated electronic transitions for  $\text{A6}^{\bullet+}$ . (B) Transient absorption spectra observed at 1  $\mu\text{s}$  ( $\square$ ), 16  $\mu\text{s}$  ( $\circ$ ), and 1 ms ( $\triangle$ ) after pulse irradiation of Ar-saturated 1,2-DCE solution containing  $10^{-4}$  M of A6. Insets: time profiles of the transient at different wavelengths.

between A6 and TNCE (Figure 6A). The transient absorption spectrum recorded 16  $\mu\text{s}$  after the pulse exhibited four distinct albeit narrow absorption bands with  $\lambda_{\text{max}} = 315$ , 360, 380, and 400 nm (Figure 6B). The more intense 400 nm band was fully developed within 16  $\mu\text{s}$  with the first-order rate constant  $k = (3.6 \pm 0.02) \times 10^5$   $\text{s}^{-1}$ , which was slower than that measured for A5. With the lapse of time the spectra recorded do not change their spectral features in the vicinity of the earlier observed absorption maxima.

Similarly to 1,2-DCE solutions containing A3 and A4, the 315, 360, 380, and 400 nm bands grew further over the 500  $\mu\text{s}$  time domain.

Pulse radiolysis of  $\text{O}_2$ -saturated acetone and acetonitrile solutions containing A6 yielded absorption spectra with similar features (Figure S4A and B in the Supporting Information). The transient absorption spectra obtained at 4.8  $\mu\text{s}$  after the pulse consisted of three absorption bands of various intensities with maxima located at  $\lambda_{\text{max}} = 350$ , 380, and 400/405 nm for both acetone and acetonitrile solutions, respectively.

With the further lapse of time, the absorption spectrum in the 350–420 nm decreased in intensity; however, a red-edge shoulder in the range 430–460 nm developed within the time range 4.8–20  $\mu\text{s}$ . For both solvents the 400 and 405 nm bands were fully developed within the range of 4.8  $\mu\text{s}$  with the first-order rate constants  $k = (5.3 \pm 0.5) \times 10^5$  and  $k = (5.4 \pm 0.2) \times 10^5$   $\text{s}^{-1}$  for acetone and acetonitrile, respectively (left insets in Figure S4A and B in the Supporting Information). On the other hand, the 430 nm band was fully developed within the range of 8  $\mu\text{s}$  with the first-order rate constants  $k = (1.3 \pm 0.4) \times 10^5$  and  $k = (3.0 \pm 0.2) \times 10^5$   $\text{s}^{-1}$  for acetone and acetonitrile,

**Table 1. Pseudo-First-Order Rate Constants for the Formation of Radical Cations ( $A^{*+}$ ) and Dimeric Radical Cations ( $A_2^{*+}$ ) (in Italic), Derived from  $10^{-4}$  M Oxoisoaporphine Derivatives**

solvent	$k \times 10^{-3} \text{ s}^{-1}$					
	$A1^{*+}$ <i>(A1)<sub>2</sub><sup>*+</sup></i>	$A2^{*+}$ <i>(A2)<sub>2</sub><sup>*+</sup></i>	$A3^{*+}$ <i>(A3)<sub>2</sub><sup>*+</sup></i>	$A4^{*+}$ <i>(A4)<sub>2</sub><sup>*+</sup></i>	$A5^{*+}$ <i>(A5)<sub>2</sub><sup>*+</sup></i>	$A6^{*+}$ <i>(A6)<sub>2</sub><sup>*+</sup></i>
1,2-DCE	5.6 ± 0.25	2.1 ± 0.03	2.3 ± 0.05	4.2 ± 0.07	15 ± 0.4	3.6 ± 0.02
acetone	2.2 ± 0.6	5.8 ± 0.7	4.5 ± 1.4	6.7 ± 2.9	11 ± 1	5.3 ± 0.5
	nm	nm	nm	nm	<b>2.7 ± 0.6</b>	<b>1.3 ± 0.4</b>
acetonitrile	3.8 ± 0.04 <sup>a</sup>	4.6 ± 0.09 <sup>a</sup>	5.7 ± 0.2	7.8 ± 2.7 <sup>c</sup>	9.8 ± 0.3	5.4 ± 0.2
				9.4 ± 4.8 <sup>d</sup>	(7.9 ± 0.06) <sup>b</sup>	(5.1 ± 0.05) <sup>b</sup>
	<b>0.85 ± 0.04<sup>a</sup></b>	<b>1.1 ± 0.1<sup>a</sup></b>	<b>1.6 ± 0.04</b>	<b>1.3 ± 0.02</b>	<b>3.2 ± 0.3</b>	<b>3.0 ± 0.2</b>
					<b>(0.41 ± 0.06)<sup>b</sup></b>	<b>(0.11 ± 0.01)<sup>b</sup></b>

<sup>a</sup>Reference 26; nm = not measured. <sup>b</sup>Bimolecular rate constants  $\times 10^9 \text{ M}^{-1} \text{ s}^{-1}$  (Supporting Information). The bimolecular rate constant can be estimated as the pseudo-first-order rate constant/ $[A]_0$ . <sup>c</sup>At 400 nm. <sup>d</sup>At 370 nm.

**Table 2. Rate Constants for the Decay of Radical Cations ( $A^{*+}$ ) and Dimeric Radical Cations ( $A_2^{*+}$ ) (Italic) Derived from Oxoisoaporphine Derivatives**

solvent	$k \times 10^{-4} \text{ s}^{-1}$					
	$A1^{*+}$ <i>(A1)<sub>2</sub><sup>*+</sup></i>	$A2^{*+}$ <i>(A2)<sub>2</sub><sup>*+</sup></i>	$A3^{*+}$ <i>(A3)<sub>2</sub><sup>*+</sup></i>	$A4^{*+}$ <i>(A4)<sub>2</sub><sup>*+</sup></i>	$A5^{*+}$ <i>(A5)<sub>2</sub><sup>*+</sup></i>	$A6^{*+}$ <i>(A6)<sub>2</sub><sup>*+</sup></i>
acetone	1.4 ± 0.08	2.7 ± 0.05	4.3 ± 0.15	4.7 ± 0.6	5.1 ± 0.2	3.3 ± 0.07
	nm	nm	nm	nm	<b>1.5 ± 0.07</b>	<b>1.9 ± 0.2</b>
acetonitrile	1.3 ± 0.03	1.1 ± 0.01	2.7 ± 0.06	<i>a</i>	4.4 ± 0.1	2.3 ± 0.05
	<b>0.5 ± 0.01</b>	<b>0.5 ± 0.02</b>	<b>0.82 ± 0.02</b>	<i>a</i>	<b>0.67 ± 0.06</b>	<b>1.6 ± 0.1</b>

<sup>a</sup>Ground depletion observed at long time; nm = rate constant not measured.

respectively (right insets in Figure 9A and B in the Supporting Information).

In acetone, the 400 nm band decayed by a first-order process with  $k = (3.3 \pm 0.07) \times 10^4 \text{ s}^{-1}$ , and a delayed decay of the 430 nm absorption was observed with  $k = (1.9 \pm 0.2) \times 10^4 \text{ s}^{-1}$  (right inset in Figure S4A in the Supporting Information). On the other hand, in acetonitrile, the 405 nm band decayed by a first-order process with  $k = (2.3 \pm 0.05) \times 10^4 \text{ s}^{-1}$ , and a delayed decay of the 430 nm absorption was observed with  $k = (1.6 \pm 0.1) \times 10^4 \text{ s}^{-1}$  (right inset in Figure S4B in the Supporting Information). Again, a close inspection of the spectra in acetone and acetonitrile shows that the ratio  $r = G\epsilon_{400/405}/G\epsilon_{430}$  calculated at 4.8, 20, 40, and 100  $\mu\text{s}$  was not constant. These observations are consistent with the existence of two radical cationic species derived from  $A6$ ,  $A6^{*+}$  and  $(A6)_2^{*+}$ , however, with a lower efficiency in acetone. The absorption of this dimeric radical cation was reproduced fairly well by the quantum mechanical calculations.

## CONCLUSIONS

Experimental data as well as theoretical spectral calculations for oxoisoaporphine derivatives (OIA) show unequivocally that the oxoisoaporphines radical cations can be formed in thermally induced electron-transfer reactions with a suitable electron acceptor, TCNE (eq 21).



The radical cations of oxoisoaporphines are mostly characterized by absorption maxima of the most intense bands located at  $\lambda_{\text{max}} = 400\text{--}410 \text{ nm}$ , except for the radical cations derived from 2,3-dihydrooxoisoaporphines. For these compounds, the absorption maxima of the most intense absorption bands were located at  $\lambda_{\text{max}} = 290\text{--}295 \text{ nm}$  (Supporting Information, Table S1). Their locations were

independent of the presence of functional groups and the solvents used. These absorbing species were formed in bimolecular processes (eq 22) with the pseudo-first-order rate constants ranging from  $2.1 \times 10^5$  to  $1.5 \times 10^6 \text{ s}^{-1}$ , Table 1, depending on the derivative and the solvent (S) used.



In acetone and acetonitrile the transient species decayed predominantly by a first-order kinetics with the first-order rate constants ranging from  $1.1 \times 10^4$  to  $5.1 \times 10^4 \text{ s}^{-1}$  (Table 2), although they were nearly stable in 1,2-dichloroethane and very stable in the thermal reaction with TCNE.

The time evolution of transient spectra and kinetic behavior at various wavelengths strongly suggest that, at relatively low concentrations of oxoisoaporphines ( $10^{-4} \text{ M}$ ), the radical cations derived from all oxoisoaporphines studied underwent aggregation with the oxoisoaporphine ground states in acetonitrile and those derived from the azaoxoisoaporphines additionally in acetone (eq 23).



The dimeric radical cations were characterized by absorption bands with maxima that were red-shifted by  $\sim 50\text{--}100 \text{ nm}$  (relative to the monomeric radical cations) (Table S1, Supporting Information). Interestingly, such an aggregation did not occur in Ar-saturated 1,2-dichloroethane.

The position of the absorption maxima and the respective oscillator strengths for the radical cations were calculated for the "isolated" species, disregarding any solvent effect. Nonetheless, they fit nicely to the experimental spectra as far as the relative position of the absorption maxima and the oscillator strengths are concerned. Some discrepancies observed, with respect to the experimental and calculated absorption maxima, can be rationalized by the solvent Stokes shifts effect.

The results of this study suggest that these oxoisoaporphines working as phytoalexins, besides a photochemical component operating in the presence of oxygen and light, may have a thermal role that operates in the dark in the presence of a suitable electron acceptor.

## ■ ASSOCIATED CONTENT

### ■ Supporting Information

Selected transient absorption spectra in pulse-irradiated 1,2-DCE, acetone, and acetonitrile solutions containing A1, A4, A5, and A6; kinetic constants at different A5/A6 concentrations; and absorption wavelength summary table. This material is available free of charge via the Internet at <http://pubs.acs.org>.

## ■ AUTHOR INFORMATION

### Corresponding Authors

\*J. R. De la Fuente: e-mail, [jrfuente@ciq.uchile.cl](mailto:jrfuente@ciq.uchile.cl).

\*K. Bobrowski: e-mail, [k.bobrowski@ichtj.waw.pl](mailto:k.bobrowski@ichtj.waw.pl).

### Notes

The authors declare no competing financial interest.

## ■ ACKNOWLEDGMENTS

Helpful comments of Dr. Gordon L. Hug (NDRL) are deeply appreciated. We thank Dr. Eduardo Sobarzo-Sanchez (USC) for the samples of oxoisoaporphines and the FONDECYT Grants Nos. 1100121, 1070623, and 7080096 for financial support that made possible short exchange visits of J.R.F. and K.B. in the INCT (Warsaw, Poland) and the Universidad de Chile (Santiago, Chile), respectively. C.A. thanks CONICYT for the Ph.D. fellowship, Project No. 24091001, and the final Fellowship to write the Doctoral Thesis and Universidad de Chile for the Travel Grant that made possible his 3 month visit in the INCT (Warsaw, Poland) to perform pulse radiolysis experiments.

## ■ REFERENCES

- (1) Flors, C.; Santi Nonell, S. Light and Singlet Oxygen in Plant Defense Against Pathogens: Phototoxic Phenalenone Phytoalexins. *Acc. Chem. Res.* **2006**, *39*, 293–300.
- (2) Flors, C.; Ogilby, P. R.; Luis, J. G.; Grillo, T. A.; Izquierdo, L. R.; Gentili, P. L.; Bussotti, L.; Nonell, S. Phototoxic Phytoalexins. Processes that Compete with the Photosensitized Production of Singlet Oxygen by 9-phenylphenalenones. *Photochem. Photobiol.* **2006**, *82*, 95–103.
- (3) Marti, C.; Jurgens, O.; Cuenca, O.; Casals, M.; Nonell, S. Aromatic Ketones as Standards for Singlet Molecular Oxygen  $O_2(^1\Delta_g)$  Photosensitization. Time-resolved photoacoustic and NIR emission studies. *J. Photochem. Photobiol. A: Chem.* **1996**, *97*, 11–18.
- (4) Schmidt, R.; Tanielian, C.; Dunsbach, R.; Wolff, C. Phenalenone, a Universal Reference Compound for the Determination of Quantum Yields of Singlet Oxygen  $O_2(^1\Delta_g)$  Sensitization. *J. Photochem. Photobiol. A: Chem.* **1994**, *79*, 11–17.
- (5) Chang, F. R.; Wei, J. L.; Teng, C. M.; Wu, Y. C. Antiplatelet Aggregation Constituents from *Annona Purpurea*. *J. Nat. Prod.* **1998**, *61*, 1457–1461.
- (6) Chen, Y. Y.; Chang, F. R.; Wu, Y. C. Isoquinoline Alkaloids and Ligands from *Rollinia Mucosa*. *J. Nat. Prod.* **1996**, *59*, 904–906.
- (7) Chen, K. S.; Chang, F. R.; Chia, Y. C.; Wu, T. S.; Wu, Y. C. Chemical Constituents of *Neolitsea Parvigemma* and *Neolitsea Konishii*. *J. Chin. Chem. Soc.* **1998**, *45*, 103–110.
- (8) Chen, C. L.; Chang, H. M.; Cowling, E. B.; Huang Hsu, C. Y.; Gates, R. P. Aporphine Alkaloids and Ligands Formed in Response to Injury of Sapwood in *Liriodendron Tulipifera*. *Phytochemistry* **1976**, *15*, 1161–1167.

(9) Blanco, O. M.; Castedo, L.; Villaverde, M. C. Alkaloids from *Platycapnos Spicata*. *Phytochemistry* **1993**, *32*, 1055–1057.

(10) Tojo, E.; Dominguez, D.; Castedo, L. Alkaloids from *Sarcopnos Enneaphylla*. *Phytochemistry* **1991**, *30*, 1005–1010.

(11) Killmer, L.; Vogt, F. G.; Freyer, A. J.; Menachery, M. D.; Adelman, C. M. Lakshminine, a New Rare Oxoisoaporphine Alkaloid from *Sciadotenia Toxifera*, and Structural Revisions of Telazolone and Teladiazolone, two Related Oxoaporphines from *Telotoxicum Peruvianum* and *T-glaziovii*. *J. Nat. Prod.* **2003**, *66*, 115–118.

(12) Yu, B. W.; Meng, L. H.; Chen, J. Y.; Zhou, T. X.; Cheng, K. F.; Ding, J.; Qin, G. W. Cytotoxic Oxoisoaporphine Alkaloids from *Menispermum Dauricum*. *J. Nat. Prod.* **2001**, *64*, 968–970.

(13) Sugimoto, Y.; Babiker, H. A. A.; Inanaga, S.; Kato, M.; Isogai, A. Oxoisoaporphines from *Menispermum Dauricum*. *Phytochemistry* **1999**, *52*, 1431–1435.

(14) Ohiri, F. C.; Verpoorte, R.; Svendsen, A.; Baerheim, A. Alkaloids from *Chasmanthera Dependens*. *Planta Med.* **1982**, *46*, 228–230.

(15) Aynur, S. Alkaloids from *Glaucium Leiocarpum*. *Planta Med.* **1999**, *65*, 492.

(16) Orahovats, A. S.; Dutschewska, H. B.; Mollow, N. M. Photochemical Oxidation of Glauicine. *Dokl. Bolg. Akad. Nauk* **1973**, *26*, 491–492.

(17) Flors, C.; Prat, C.; Suau, R.; Najera, F.; Nonell, S. Photochemistry of Phytoalexins Containing Phenalenone-like Chromophores: Photophysics and Singlet Oxygen Photosensitizing Properties of the Plant Oxoaporphine Alkaloid Oxoglauicine. *Photochem. Photobiol.* **2005**, *81*, 120–124.

(18) Zanicco, A. L.; Lemp, E.; Gunther, G. A Kinetic Study of the Reaction Between Boldine and Singlet Oxygen [ $O_2(^1\Delta_g)$ ]. *J. Chem. Soc., Perkin Trans.* **1997**, *2*, 1299–1302.

(19) Towers, G. H. N.; Page, J. E.; Hudson, J. B. Light-mediated Biological Activities of Natural Products from Plants and Fungi. *Curr. Org. Chem.* **1997**, *1*, 395–414.

(20) Bu, X.; Chen, J.; Deady, L. W.; Smith, C. L.; Baguley, B. C.; Greenhalgh, D.; Yang, S.; Denny, W. A. Synthesis and Cytotoxic Activity of N-[(alkylamino)alkyl]carboxamide Derivatives of 7-oxo-7H-benz[De]anthracene, 7-oxo-7H-naphtho[1,2,3-de]quinoline, and 7-oxo-7H-benzo[e]perimidine. *Bioorg. Med. Chem.* **2005**, *13*, 3657–3665.

(21) Borovlev, I. V.; Demidov, O. P.; Aksenov, A. V.; Pozharskii, A. F. Heterocyclic Analogs of Pleiadiene: LXXIV. Peri-cyclizations in the Perimidine Series. Synthesis of 1,3-diazapyrene Derivatives. *Russ. J. Org. Chem.* **2004**, *40*, 895–901.

(22) Dzieduszycka, M.; Martelli, S.; Arciemiuik, M.; Bontemps-Gracz, M. M.; Kupiec, A.; Borowski, E. Effect of Modification of 6-[(Aminoalkyl)amino]-7H-benzo[e]perimidin-7-ones on Their Cytotoxic Activity Toward Sensitive and Multidrug Resistant Tumor Cell Lines. Synthesis and Biological Evaluation. *Bioorg. Med. Chem.* **2002**, *10*, 1025–1035.

(23) Stefanska, B.; Dzieduszycka, M.; Bontemps-Gracz, M. M.; Borowski, E.; Martelli, S.; Supino, R.; Pratesi, G.; De Cesare, M.; Zunino, F.; Kusnierczyk, H.; Radzikowski, C. 8,11-Dihydroxy-6-[(aminoalkyl)amino]-7H-benzo[e]perimidin-7-ones with Activity in Multidrug-resistant Cell Lines: Synthesis and Antitumor Evaluation. *J. Med. Chem.* **1999**, *42*, 3494–3501.

(24) Stefanska, B.; Dzieduszycka, M.; Martelli, S.; Tarasiuk, J.; Bontempsgracz, M.; Borowski, E. 6-[(Aminoalkyl)Amino]-Substituted 7H-Benzo[E]Perimidin-7-Ones as Novel Antineoplastic Agents - Synthesis and Biological Evaluation. *J. Med. Chem.* **1993**, *36*, 38–41.

(25) De la Fuente, J. R.; Aliaga, C.; Poblete, C.; Zapata, G.; Jullian, C.; Saitz, C.; Cañete, A.; Kciuk, G.; Sobarzo-Sánchez, E.; Bobrowski, K. Photoreduction of Oxoisoaporphines by Amines: Laser Flash and Steady-State Photolysis, Pulse Radiolysis, and TD-DFT Studies. *J. Phys. Chem. A* **2009**, *113*, 7737–7747.

(26) De la Fuente, J. R.; Kciuk, G.; Sobarzo-Sanchez, E.; Bobrowski, K. Transient Phenomena in the Pulse Radiolysis of Oxoisoaporphine Derivatives in Acetonitrile. *J. Phys. Chem. A* **2008**, *112*, 10168–10177.

(27) De la Fuente, J. R.; Aliaga, C.; Cañete, A.; Kciuk, G.; Szreder, T.; Bobrowski, K. Photoreduction of Azaoxoisoaporphines by Amines:

Laser Flash and Steady-State Photolysis and Pulse Radiolysis Studies. *Photochem. Photobiol.* **2013**, *89*, 1417–1426.

(28) Aliaga, C.; Cerón-Neculpán, M.; Saitz, C.; Jullian, C.; Sobarzo-Sánchez, E.; De la Fuente, J. R. Oxoisoaporphines: Regioselective Deuterium Labelling Involving the Metastable Hydrogenated Photo-product Anions. *J. Photochem. Photobiol. A* **2011**, *222*, 360–365.

(29) De la Fuente, J. R.; Neira, V.; Saitz, C.; Jullian, C.; Sobarzo-Sánchez, E. Photoreduction of Oxoisoaporphine Dyes by Amines: Transient-absorption and Semiempirical Quantum-Chemical Studies. *J. Phys. Chem. A* **2005**, *109*, 5897–5904.

(30) De la Fuente, J. R.; Jullian, C.; Saitz, C.; Sobarzo-Sánchez, E.; Neira, V.; Gonzalez, C.; Lopez, R.; Pessoa-Mahana, H. Photoreduction of Oxoisoaporphines. Another Example of a Formal Hydride-Transfer Mechanism. *Photochem. Photobiol. Sci.* **2004**, *3*, 194–199.

(31) Rathore, R.; Lindeman, S. V.; Kochi, J. K. Charge-Transfer Probes for Molecular Recognition via Steric Hindrance in Donor-Acceptor Pairs. *J. Am. Chem. Soc.* **1997**, *119*, 9393–9404.

(32) Laatsch, H.; Sigel, C.; Kral, A. Measurement of the Donor Strength of Substituted 1-Naphthols. *Chem. Ber.* **1994**, *127*, 393–400.

(33) Yan, B. Z.; Zhang, Z. G.; Yuan, H. C.; Wang, L. C.; Xu, J. H. Photoinduced Electron Transfer Reactions of Chloranil with Benzodioxoles. *J. Chem. Soc., Perkin Trans.* **1994**, *2*, 2545–2550.

(34) Maslak, P.; Chapman, W. H. Mesolytic Scission of C-C Bonds as a Probe for Photoinduced Electron Transfer Reactions of Quinones. *J. Org. Chem.* **1996**, *61*, 2647–2656.

(35) Di Bella, S.; Fragala, I. L.; Ratner, M. A.; Marks, T. J. Electron Donor-Acceptor Complexes as Potential High-Efficiency Second-Order Nonlinear Optical Materials. A Computational Investigation. *J. Am. Chem. Soc.* **1993**, *115*, 682–686.

(36) Perrier, S.; Sankararaman, S.; Kochi, J. K. Photoinduced Electron-Transfer in Pinacol Cleavage with Quinones via Highly Labile Cation Radicals - Direct Comparison of Charge-Transfer Excitation and Photosensitization. *J. Chem. Soc., Perkin Trans.* **1993**, *2*, 825–837.

(37) Sun, D.; Rosokha, S. V.; Kochi, J. K. Reversible Interchange of Charge-Transfer Versus Electron-Transfer States in Organic Electron Transfer via Cross-Exchanges Between Diamagnetic (Donor/Acceptor) Dyads. *J. Phys. Chem. B* **2007**, *111*, 6655–6666.

(38) Reddy, A. R.; Krishnamurthy, N. V.; Bhudevi, B. Molecular Adducts Between a Few Phenolic Donors and Pi-Acceptors in Solid-State. *Spectrosc. Acta Pt. A-Mol. Biomol. Spectrosc.* **2006**, *63*, 700–708.

(39) Bobrowski, K. Radiation Induced Radical Reactions. In *Encyclopedia of Radicals in Chemistry, Biology and Materials*; Chatgililoglu, C.; Studer, A., Eds.; John Wiley&Sons Ltd.: New York, 2012; pp 1–38.

(40) Fabre, J. L.; Farge, D.; James, C. Dibenzo[de,h]quinoline Derivatives. Patent No. US4,128,650, 1978.

(41) Walker, G. N.; Kempton, R. J. Aromatic Demethoxylation in the Cyclization of 3-( $\beta$ -dialkoxyarylethylamino)phthalides to 2,3-Dihydro-7H-dibenzo[da,h]quinolines. *J. Org. Chem.* **1971**, *36*, 1413–1416.

(42) Sobarzo-Sánchez, E.; De la Fuente, J.; Castedo, L. Synthesis and Total Assignment of H-1 and C-13 NMR Spectra of New Oxoisoaporphines by Long-Range Heteronuclear Correlations. *Magn. Reson. Chem.* **2005**, *43*, 1080–1083.

(43) Sobarzo-Sánchez, E.; Cassels, B. K.; Castedo, L. An Expedient Synthesis of Unusual Oxoisoaporphine and Annelated Quinoline Derivatives. *Synlett.* **2003**, 1647–1650.

(44) Sobarzo-Sánchez, E. Síntesis y Reactividad en el Ámbito de las 7H-Dibenzo[de,h]quinolinas. *Ph.D. Thesis*. Universidad de Chile, Santiago, Chile, 2003.

(45) Nicolet, O.; Banerji, N.; Pagès, S.; Vauthey, E. Effect of the Excitation Wavelength on the Ultrafast Charge Recombination Dynamics of Donor - Acceptor Complexes in Polar Solvents. *J. Phys. Chem. A* **2005**, *109*, 8236–8245.

(46) Ganesan, V.; Rosokha, S. V.; Kochi, J. K. Isolation of the Latent Precursor Complex in Electron-Transfer Dynamics. Intermolecular Association and Self-Exchange with Acceptor Anion Radicals. *J. Am. Chem. Soc.* **2003**, *125*, 2559–2571.

(47) Zhou, J. W.; Findley, B. R.; Teslja, A.; Braun, C. L.; Sutin, N. Ion Pairs from Photoexcited, "Random" Electron Donors and Acceptors:

Alkylbenzenes and Tetracyanoethylene. *J. Phys. Chem. A* **2000**, *104*, 11512–11521.

(48) Hilinski, E. F.; Masnovi, J. M.; Kochi, J. K.; Rentzepis, P. M. Role of Ion Pairs in the Photochemistry of Electron Donor-Acceptor Complexes. Picosecond Spectroscopic Studies of Arene-Tetracyanoethylene systems. *J. Am. Chem. Soc.* **1984**, *106*, 8071–8077.

(49) Fujitsuka, M.; Ito, O.; Dragoe, N.; Ito, S.; Shimotani, H.; Takagi, H.; Kitazawa, K. Photophysical and Photochemical Processes of an Unsymmetrical Fullerene Dimer, C121. *J. Phys. Chem. B* **2002**, *106*, 8562–8568.

(50) Haga, N.; Nakajima, H.; Takayanagi, H.; Tokumaru, K. Photoinduced Electron Transfer Between Acenaphthylene and Tetracyanoethylene: Effect of Irradiation Mode on Reactivity of the Charge-Transfer Complex and the Resulted Radical Ion Pair in Solution and Crystalline State. *J. Org. Chem.* **1998**, *63*, 5372–5384.

(51) Gumy, J. C.; Vauthey, E. Investigation of the Excited-State Dynamics of Radical Ions in the Condensed Phase Using the Picosecond Transient Grating Technique. *J. Phys. Chem. A* **1997**, *101*, 8575–8580.

(52) Evans, C. H.; Scaiano, J. C. Photochemical Generation of Radical Cations from  $\alpha$ -Terthienyl and Related Thiophenes: Kinetic Behavior and Magnetic Field Effects on Radical-Ion Pairs in Micellar Solution. *J. Am. Chem. Soc.* **1990**, *112*, 2694–2701.

(53) Rosokha, S. V.; Newton, M. D.; Head-Gordon, M.; Kochi, J. K. Mulliken-Hush Elucidation of the Encounter (precursor) Complex in Intermolecular Electron Transfer via Self-Exchange of Tetracyanoethylene Anion-Radical. *Chem. Phys.* **2006**, *324*, 117–128.

(54) Sofue, M.; Nagakura, S. The Formation of the Anion Radicals of Pyromeritonitrile and Tetracyanoethylene by Flash Irradiation. *Bull. Chem. Soc. Jpn.* **1965**, *38*, 1048–1049.

(55) Rosokha, S. V.; Kochi, J. K. Continuum of Outer- and Inner-Sphere Mechanisms for Organic Electron Transfer, Steric Modulation of the Precursor Complex in Paramagnetic (Ion-Radical) Self-Exchanges. *J. Am. Chem. Soc.* **2007**, *129*, 3683–3697.

(56) Rosokha, S. V.; Newton, M. D.; Jalilov, A. S.; Kochi, J. K. The Spectral Elucidation versus the X-ray Structure of the Critical Precursor Complex in Bimolecular Electron Transfers: Application of Experimental/Theoretical Solvent Probes to Ion-Radical (Redox) Dyads. *J. Am. Chem. Soc.* **2008**, *130*, 1944–1952.

(57) Lu, J.-M.; Rosokha, S. V.; Kochi, J. K. Stable (long-bonded) Dimers via the Quantitative Self-Association of Different Cationic, Anionic, and Uncharged pi-radicals: Structures, Energetics, and Optical Transitions. *J. Am. Chem. Soc.* **2003**, *125*, 12161–12171.

(58) Chang, R. Dimerization of Tetracyanoethylene Anion Radical. *J. Phys. Chem.* **1970**, *74*, 2029–2030.

(59) Bobrowski, K. Free Radicals in Chemistry, Biology, and Medicine: Contribution of Radiation Chemistry. *Nukleonika* **2005**, *50* (Supplement 3), S67–S76.

(60) Mirkowski, J.; Wisniewski, P.; Bobrowski, K. *INCT Annual Report 2000*; INCT: Warsaw, 2001; pp 31–33.

(61) Wang, Y.; Tria, J. J.; Dorfman, L. M. Identity and Yield of Positive Charge Centers in Irradiated Chloro Hydrocarbon Liquids and the Rates of their Interaction with Solute Molecules. *J. Phys. Chem.* **1979**, *83*, 1946–1951.

(62) Baptista, J. L.; Burrows, H. D. Solute Ion and Radical Formation in the Pulse Radiolysis of Acetonitrile Solutions. *J. Chem. Soc., Faraday Trans. 1* **1974**, *70*, 2066–2079.

(63) Singh, A.; Gesser, H. D.; Scott, A. R. Solvated Electron in Acetonitrile. *Chem. Phys. Lett.* **1968**, *2*, 271–273.

(64) Hayon, E. Yield of Ions and Excited States Produced in the Radiolysis of Polar Organic Liquids. *J. Chem. Phys.* **1970**, *53*, 2353–2358.

(65) Bell, I. P.; Rodgers, M. A. J.; Burrows, H. D. Kinetic and Thermodynamic Character of Reducing Species Produced on Pulse Radiolysis of Acetonitrile. *J. Chem. Soc., Faraday Trans. 1* **1977**, *73*, 315–326.

(66) Vedenev, V. I.; Gurvich, L. V.; Kondrat'yev, V. N.; Medvedev, V. A.; Frankevich, Y. L. *Bond Energies, Ionization Potentials and Electron Affinities*; Edward Arnold Ltd.: London, 1966.

- (67) Rodgers, M. A. J. Nanosecond Pulse Radiolysis of Acetone. *J. Chem. Soc., Faraday Trans. 1* **1972**, *68*, 1278–1286.
- (68) Rodgers, M. A. J. Pulse Radiolysis Studies of Acetone Solutions. *J. Chem. Soc., Faraday Trans. 1* **1971**, *67*, 1029–1040.
- (69) Arai, S.; Kira, A.; Imamura, M. Pulse Radiolysis Studies of Acetone Solutions of Biphenyl and Anthracene: Formation of Ions and Excited Singlet State. *J. Chem. Phys.* **1971**, *54*, 5073–5081.
- (70) El Omar, A. K.; Schmidhammer, U.; Pernot, P.; Murata, S.; Mostafavi, M. Picosecond Pulse Radiolysis Study on the Distance Dependent Reaction of the Solvated Electron with Organic Molecules in Ethylene Glycol. *J. Phys. Chem. A* **2012**, *116*, 11989–11996.
- (71) Robinson, A. J.; Rodgers, M. A. J. Primary Processes in Acetone Radiolysis. *J. Chem. Soc., Faraday Trans. 1* **1973**, *69*, 2036–2045.